Proceedings of the ASME 2012 International Design Engineering Technical Conferences & Computers and Information in Engineering Conference
IDETC/CIE 2012
August 12-15, 2012, Chicago, IL, USA

DETC2012-71182

VEHICLE STABILITY CONTROL THROUGH PREDICTIVE AND OPTIMAL TIRE SATURATION MANAGEMENT

Justin Sill
Clemson University – International Center for Automotive Research
Greenville, SC

Beshah Ayalew
Clemson University – International Center for Automotive Research
Greenville, SC

ABSTRACT

This paper presents a predictive vehicle stability control (VSC) strategy that distributes the drive/braking torques to each wheel of the vehicle based on the optimal exploitation of the available traction capability for each tire. To this end, tire saturation levels are defined as the deficiency of a tire to generate a force that linearly increases with the relevant slip quantities. These saturation levels are then used to set up an optimization objective for a torque distribution problem within a novel cascade control structure that exploits the natural time scale separation of the slower lateral handling dynamics of the vehicle from the relatively faster rotational dynamics of the wheel/tire.

The envisaged application of the proposed vehicle stability strategy is for vehicles with advanced and emerging pure electric, hybrid electric or hydraulic hybrid power trains featuring independent wheel drives. The developed predictive control strategy is evaluated for, a two-axle truck featuring such an independent drive system and subjected to a transient handling maneuver.

Key words: Vehicle stability control, tire saturation, predictive vehicle control, torque management, independent drives

INTRODUCTION

The adoption of vehicle stability control (VSC) systems have been instrumental in reducing fatalities in single-vehicle crashes [1, 2]. VSC (also called vehicle dynamics control (VDC) or electronic stability control (ESC)) systems help in reducing accidents by maintaining a driver's control of the vehicle during emergency/aggressive maneuvers that approach or exceed the limits of tire/road adhesion. Most VSC systems available on commercial vehicles today control the vehicle through active individual wheel braking by extending the existing hardware previously developed for anti-lock braking (ABS) and traction control systems. These current VSC systems use differential (left-to-right) braking on either the front or rear axle based on a set of pre-defined rules and thresholds to generate a required corrective yaw moment for stabilization or for achieving the intentions of the driver steering inputs [1, 3].

There exists an opportunity to integrate stability control strategies that use alternative methods of activation as demonstrated by previous researchers utilizing controller corrections on front and rear steering [4-6], varying degrees of traction management [7-9], as well as active and semi-active suspension elements [10, 11].

This paper specifically focuses on predictive stability control for advanced and emerging vehicles with powertrains incorporating independently controlled wheel drives. These power trains could offer increased energy efficiency and reliability as well as improved packaging and noise/vibration isolation benefits. In this paper, however, we exploit the ability of applying independent torques to each wheel of the vehicle to design a novel torque distribution control strategy that can be used to ensure stability and driver-intended performance while targeting optimal use of available tire traction capability.

Defining Saturation

The interaction between a tire and the road surface has inherent nonlinearities and inefficiencies due to frictional adhesion limits. We refer to the main behavior as tire saturation and construct a metric to quantify the saturation level by comparing the actual nonlinear tire behavior to a linear expectation. The saturation level characterizes the deficiency of a tire to generate a force that increases linearly with slip. As depicted in Figure 1, for a typical tire, as the saturation level increases, the traction capacity of the tire decreases.

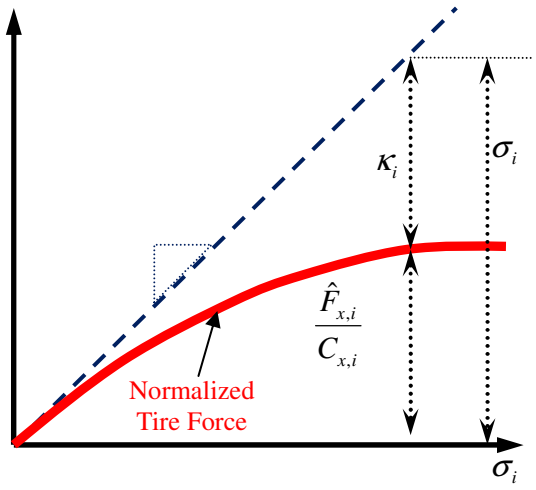

Figure 1. Tire Force Saturation

The longitudinal tire force saturation can be defined mathematically as:

$$\kappa_i = \sigma_i - \frac{\hat{F}_{x,i}}{C_{x,i}} \qquad (1)$$

where, σ_i is the tire slip ratio; and $\hat{F}_{x,i}$ is the (estimate of) instantaneous longitudinal tire force; and $C_{x,i}$ is the tire slip stiffness, assumed to be constant. Similar definitions can be given for the lateral tire force saturations as we do in our previous work [12]. In this paper, we refer only to longitudinal tire force saturations.

A previous work in [13] treated the presence of lateral tire force saturation as an undesirable state to be merely detected and avoided with abrupt braking intervention to the saturated tire. No provision was made to quantify and manage saturation levels, In this work we present here, a control strategy is designed to optimally balance longitudinal tire saturation levels among all tires by managing the distribution of individual drive/brake torques.

Model Predictive Control

We propose and demonstrate a predictive control strategy to balance the impending tire saturation levels through controlled torque interventions within an optimal framework. Such predictive techniques, referred to as Model Predictive Control (MPC) or specifically Nonlinear Model Predictive Control (NLMPC), have been used for vehicle control in traction control systems [14], autonomous vehicle control [15-17], and to determine under and over-steer vehicle conditions [18, 19]. However, no research yet exists on the implementation of MPC or NLMPC for torque distribution control for VSC systems that target tire saturation management in the manner proposed and addressed in this work.

Predictive control has been successfully applied to many applications in the chemical industry and in many manufacturing processes [20-23]. The basic mechanisms of MPC are shown in Figure 2. The current time in Figure 2 is denoted by index k, while the immediate past and future time indices are represented by k-1 and k+1, respectively. The horizon, H_p, defines the time range in which the predicted state is optimized by variations of the future control inputs during the control horizon, H_c.

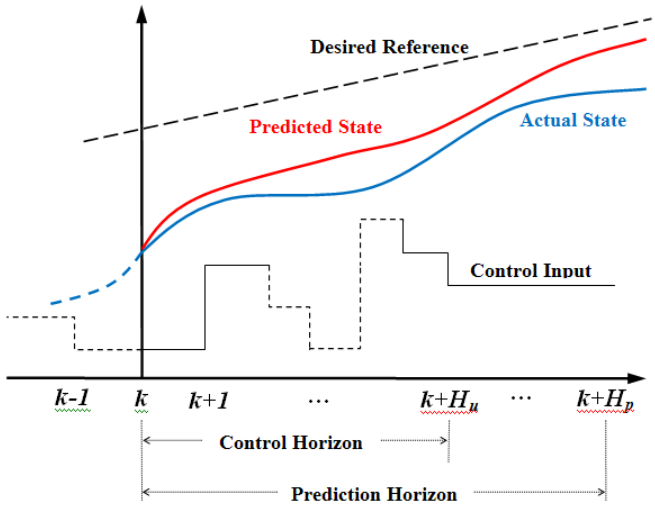

Figure 2. Illustration of Model Predictive Control

In particular, we adopt the NLMPC process, which proceeds with linearization and discretization of a predictive model, an analytical forward prediction, setting up an objective function, and finally executing an optimization solver to determine the control inputs. The reader is referred to the text by [21] for details of the NLMPC process.

Model predictive control strategies offer the possibility of explicit consideration of optimality (in some sense) and easy formulation for multiple input/multiple output (MIMO) systems. These advantages make them particularly suitable for control of advanced powertrains that have known issues of over-actuation and nonlinear behavior as recognized and addressed by previous research on vehicle control [16, 24, 25].

PREDICTIVE TORQUE DISTRIBUTION CONTROL

The structure of the proposed predictive control system is selected as a cascading of the already established yaw moment control (briefly included in the Appendix) and a novel predictive torque distribution control. In this cascade structure, which is depicted in Figure 3, the high level control explicitly computes the corrective yaw moment and passes it as a constraint to the low level control that determines the individual wheel torques. The low level control in turn distributes the torque in such a way as to optimize longitudinal tire force saturations. Vehicle sensors and lateral/longitudinal estimation routines provide the high and low level controllers with details on the current operating conditions of the vehicle for online linearizations and prediction initializations, discussed below.

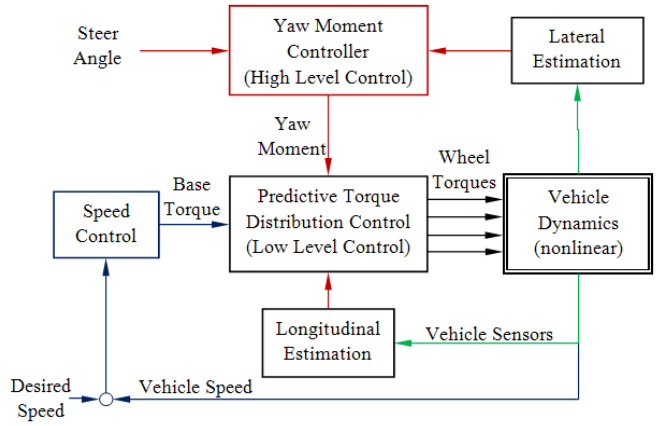

Figure 3. Yaw Moment Control Cascaded with Predictive Torque Distribution Control

This cascade structure is motivated by the observation that the system dynamics to be controlled by the high and low level controllers are of different natural time scales. The high level control must have sufficient response to control the lateral vehicle dynamics, which has a typical bandwidth in the range of 1-3 Hz. The low level control must sufficiently control the individual tire/wheel dynamics, which have higher bandwidths, in the range of 5-20 Hz. Given this basic observation, for the computations and demonstrations in this work, the predictive control application frequency is selected to be 100 Hz to sufficiently capture the fast dynamics.

Saturation Control Objective

An objective of equalizing the saturation levels can be posed by computing the deviation of the individual wheel saturations from their average using:

$$J = \left[\sum_{i=LF,RF,LR,RR} \left(\kappa_i - \frac{\sum_{j=LF,RF,LR,RR} \kappa_j}{4} \right)^2 \right] \tag{2}$$

This can be re-written in the usual quadratic matrix form as:

$$J = \begin{Bmatrix} \kappa_{LF} \\ \kappa_{RF} \\ \kappa_{LR} \\ \kappa_{RR} \end{Bmatrix}^T \left(\begin{bmatrix} 1 & 0 & 0 & 0 \\ 0 & 1 & 0 & 0 \\ 0 & 0 & 1 & 0 \\ 0 & 0 & 0 & 1 \end{bmatrix} - \frac{1}{4} \begin{bmatrix} 1 & 1 & 1 & 1 \\ 1 & 1 & 1 & 1 \\ 1 & 1 & 1 & 1 \\ 1 & 1 & 1 & 1 \end{bmatrix} \right) \begin{Bmatrix} \kappa_{LF} \\ \kappa_{RF} \\ \kappa_{LR} \\ \kappa_{RR} \end{Bmatrix} = \bar{\kappa}^T Q_1 \bar{\kappa} \tag{3}$$

where, Q_1 is a constant positive definite matrix given by the corresponding parenthesis in (3) and $\bar{\kappa}$ is a vector of the individual tire saturations.

Constraints

The torque distribution must satisfy equality constraints which are computed on-line, specifically, 1) the total base torque that is commanded by the driver (or a separate vehicle speed controller) and 2) the corrective yaw moment required by a high level controller. These constraints are represented by:

$$\begin{bmatrix} -\frac{d_f}{2R_w} & \frac{d_f}{2R_w} & -\frac{d_r}{2R_w} & \frac{d_r}{2R_w} \end{bmatrix} \begin{Bmatrix} F_{x,LF} \\ F_{x,RF} \\ F_{x,LR} \\ F_{x,RR} \end{Bmatrix} = M_\psi \tag{4}$$

$$\sum_{i=LF,RF,LR,RR} T_i = T_{total} \tag{5}$$

where, d_f and d_r are the track widths; R_w is the tire radius; $F_{x,i}$ is the individual tire forces; M_ψ is the corrective yaw moment; T_i is the individual wheel torques; and T_{total} is the total commanded drive torque.

Predictive Optimization Formulation

A key parameter of the predictive framework is the prediction horizon, which is largely dependent on the system. It is desirable to predict forward as far as possible, even to infinity. However, it is difficult to predict tire saturations for a vehicle forward to infinity, because of unknowns in the future system inputs and responses. For example, the future driver input on the vehicle cannot be known *a priori*. One only has the current inputs/constraints of yaw moment and base torque. Therefore, a simplification is made to consider a short and finite prediction horizon of 0.1 seconds to capture dynamics associated with saturation, and assume that the constraints are constant throughout this horizon. It is assumed that fast update cycles of the receding horizon control scheme (selected to be 100 Hz), which including linearization updates, offset the simplifications of short horizons and unknowable future inputs/constraints.

The instantaneous objective in (3) must be expanded throughout the prediction horizon to properly pose the MPC optimization problem:

$$\min_{\Delta U} \left(Y^T Q Y + (\Delta U)^T R (\Delta U) \right)$$

subjected to:

$$\begin{aligned} x_{k+1} &= f(x_k, u_k, \Delta u_k) \\ \bar{\kappa}_{k+1} &= g(x_{k+1}, u_k, \Delta u_k) \\ A_{eq} \Delta U &= B_{eq} \end{aligned} \tag{6}$$

$$Y = \begin{Bmatrix} \bar{\kappa}_{k+1} \\ \vdots \\ \bar{\kappa}_{k+1+H_p} \end{Bmatrix}; \quad \Delta U = \begin{Bmatrix} u_{k+1} - u_k \\ \vdots \\ u_{k+H_u} - u_k \end{Bmatrix}^T = \begin{Bmatrix} \Delta u_k \\ \vdots \\ \Delta u_{k+H_p} \end{Bmatrix}^T$$

where, the functions f and g define the predictive vehicle system model; x is the state vector of velocity, the four wheel speeds, and the four tire forces; u is the input vector of the four wheel torques and y is the output vector of the four longitudinal tire saturations. Y is a system output matrix which is a concatenation of the individual tire saturations into the future prediction horizon; A_{eq} and B_{eq} are constant matrices that define the equality constraints; Q and R are weighting matrices; and H_p is the number of steps in the prediction horizon.

The predictive model must include states governing the longitudinal dynamics of the vehicle, the dynamics of each of the four wheels, as well as longitudinal tire force dynamics. It is well known that these dynamics are nonlinear due to the definition of the wheel slip ratio, longitudinal tire force curves, and aerodynamics loads. Each of these nonlinear components are linearized (at current operating points, based on estimates) and discretized in detail derivations presented in the Appendix. The result is an equivalent discrete time system:

$$x_{k+1} = Ax_k + B_1 u_k + B_2 \tag{7}$$

$$y_k = Cx_k + E_1 \tag{8}$$

where, the matrices of A, B_1, B_2, C, and E are continuously updated for each iteration of the controller; x u, and y are as defined above. An important distinction of this process compared to standard MPC techniques [21], is the presence of constant matrices, B_2 and E_1, in (7) and (8) (See detail in Appendix).

The discretized linear system in (7) and (8) is used to analytically predict the system response as well the resulting saturations due to incremental changes in torque inputs. The expansion of the predicted response from the current to a future horizon of length H_p, is given by:

$$\begin{Bmatrix} y_k \\ y_{k+1} \\ \vdots \\ y_{k+H_p-1} \end{Bmatrix} = \begin{bmatrix} CA \\ CA^2 \\ \vdots \\ CA^{H_p} \end{bmatrix} x_k + \begin{bmatrix} CB_1 \\ CAB_1 + CB_1 \\ \vdots \\ \sum_{i=0}^{H_p-1} CA^i B_1 \end{bmatrix} u_{k-1}$$
$$+ \begin{bmatrix} CB_1 & 0 & 0 & 0 \\ CAB_1 + CB_1 & CB_1 & 0 & 0 \\ \vdots & CAB_1 + CB_1 & \ddots & 0 \\ \sum_{i=0}^{H_p-1} CA^i B_1 & \sum_{i=0}^{H_p-2} CA^i B_1 & \cdots & CB_1 \end{bmatrix} \begin{bmatrix} \Delta u_k \\ \Delta u_{k+1} \\ \vdots \\ \Delta u_{k+H_p-1} \end{bmatrix} \tag{9}$$
$$+ \begin{bmatrix} CB_2 \\ C2B_2 \\ \vdots \\ C(H_p-1)B_2 \end{bmatrix} + \begin{bmatrix} E_1 \\ E_1 \\ \vdots \\ E_1 \end{bmatrix}$$

The matrices in (9) are constructed at each control iteration with linearization updates of the prediction model. The predicted output equation, (9), can be simplified into the form:

$$Y = \gamma x_k + \Omega u_{k-1} + \zeta \Delta U + \overline{E} \tag{10}$$

where, the matrices of γ, Ω, ζ, and E are constant during one control iteration; and x_k and u_{k-1} are the current states (obtained through measurements or estimates) and previous control inputs, respectively. The analytical prediction of the output (tire saturations), Y, is substituted into the objective/cost function in (6). By expanding, simplifying, collecting terms, and neglecting constant additive terms, the cost function reduces to a quadratic form given by:

$$\min_{\Delta U} \left\{ \begin{array}{l} (\Delta U)^T \left[\zeta^T Q \zeta + R\right](\Delta U) \\ + \left[\begin{pmatrix} (\zeta x_k)^T Q + \left((\Omega u_k)^T + \overline{E}^T\right)Q \\ + (x_k \gamma Q)^T + (u_k \Omega Q)^T + (\overline{E} Q)^T \end{pmatrix} \zeta \right] \Delta U \end{array} \right\}$$
subjected to: (11)
$$A_{eq} \Delta U = B_{eq}$$

where, Q is defined by (3) for the objective of balancing saturations; and R is a diagonal of control weights that penalizes the rate of change of the input torques. The weights can be used as tuning parameters to improve the control performance. The static optimization problem in (11) can be easily solved for the wheel torque increments, ΔU, using quadratic optimization software tools.

To proceed, the equality constraint (5) should be transformed to be in terms of the control input increment for the prediction horizon. This is done through matrix expansion and inclusion of current torque inputs to present the constraint in terms of input increments as follows:

$$\sum_{i=LF,RF,LR,RR} T_i = T_{total}$$
$$\Rightarrow \begin{bmatrix} 1 & 1 & 1 & 1 \end{bmatrix} \underbrace{\{u_{k+1} - u_k\}}_{\Delta u_k} = \left[T_{total} - \sum_{i=LF,RF,LF,RR} u_{k,i} \right] \tag{12}$$
$$\Rightarrow A_{eq,1} \Delta u = B_{eq,1}$$

where, u_k is a vector of the four wheel torques; Δu_k is the increment in the input; and $u_{k,i}$ is the individual torques.

The constraint of yaw moment in (4) is more challenging to simplify for the posed optimization, because of its dependency on the tire longitudinal forces, states of the prediction model, instead of input torque increments. Therefore, this constraint can be reformulated by the substitution of the prediction model in the computation of the tire forces:

$$\begin{bmatrix} -\frac{d_f}{2R_w} & \frac{d_f}{2R_w} & -\frac{d_r}{2R_w} & \frac{d_r}{2R_w} \end{bmatrix} \{\overline{F}_x\} = M_\psi \tag{13}$$

$$\overline{F}_{x,j} = C'\left(Ax_j + B_1 u_{j-1} + B_1 \Delta u_j + B_2\right) \tag{14}$$

where, j is any indexed time; C' is an output matrix that isolates the states of individual longitudinal forces as a vector, $\overline{F}_{x,j}$.

By substitution and rearrangement, the instantaneous constraint is given by:

$$\begin{bmatrix} -\frac{d_f}{2R_w} & \frac{d_f}{2R_w} & -\frac{d_r}{2R_w} & \frac{d_r}{2R_w} \end{bmatrix} \left\{C'\left(Ax_j + B_1 u_{j-1} + B_1 \Delta u_j + B_2\right)\right\} = M_\psi$$
$$\Rightarrow \left\{ \begin{bmatrix} -\frac{d_f}{2R_w} & \frac{d_f}{2R_w} & -\frac{d_r}{2R_w} & \frac{d_r}{2R_w} \end{bmatrix} C'B_1 \right\} \Delta u_k \tag{15}$$
$$= \left\{ M_\psi - \begin{bmatrix} -\frac{d_f}{2R_w} & \frac{d_f}{2R_w} & -\frac{d_r}{2R_w} & \frac{d_r}{2R_w} \end{bmatrix} C'\left\{Ax_j + B_1 u_{j-1} + B_2\right\} \right\}$$
$$\Rightarrow A_{eq,2} \Delta u = B_{eq,2}$$

Since each equality constraint must be satisfied throughout the prediction horizon, the instantaneous definitions of (12) and

(15) are expanded for each time step in the prediction horizon as follows:

$$\begin{bmatrix} A_{eq,1} & \cdots & \bar{0} & \bar{0} & \cdots & \bar{0} \\ \vdots & \ddots & \cdots & \cdots & \cdots & \vdots \\ \bar{0} & \vdots & A_{eq,1} & \bar{0} & \cdots & \bar{0} \\ \bar{0} & \vdots & \bar{0} & A_{eq,2} & \cdots & \bar{0} \\ \vdots & \vdots & \vdots & \vdots & \ddots & \vdots \\ \bar{0} & \cdots & \bar{0} & \bar{0} & \cdots & A_{eq,2} \end{bmatrix} \Delta U = \begin{bmatrix} B_{eq,1} \\ \vdots \\ B_{eq,1} \\ B_{eq,2} \\ \vdots \\ B_{eq,2} \end{bmatrix} \Rightarrow A_{eq}\Delta U = B_{eq} \quad (16)$$

where, $A_{eq,1}$ and $B_{eq,1}$ correspond to the matrices in (12); $A_{eq,2}$ and $B_{eq,2}$ are defined by (15); and A_{eq} and B_{eq} are the equality constraints expanded throughout the prediction horizon in the posed optimization problem in (11).

As already stated, the predictive model includes many simplifying assumptions from linearization, discretization, known/unknown disturbances, short prediction horizons, and continuously changing constraints. Repeating the prediction and optimization in receding horizon control cycles (with the most recent vehicle state information every control cycle) helps compensate for these simplifications.

RESULTS & DISCUSSION

The predictive torque distribution control is applied on an example vehicle, a two-axled heavy truck, with the cascade structure already depicted in Figure 3. A yaw rate reference controller (described in the Appendix) is adopted for computing the high-level corrective moment and a PI forward speed controller determines the total base torque. The detailed equations of motion for the example heavy truck (includes seven degrees of freedom and a combined-slip tire model) to which the control is applied, can be found in previous works [12, 26, 27].

The predictive control strategy is evaluated in an open-loop transient maneuver, defined by NHTSA, to mimic an extreme lane change maneuver for purposes of VSC system testing. The steering is described by a modified sinusoid with a dwell as is shown along with a typical stable trajectory in Figure 4 (an uncontrolled vehicle becomes unstable).

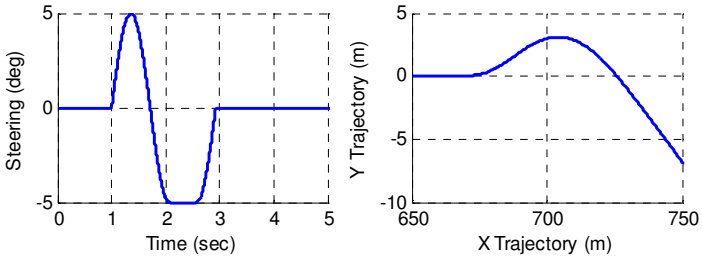

Figure 4. Road-Wheel Steer Input and Trajectory of Open-Loop Transient Maneuver

During the maneuver, the vehicle speed, initially at 80 kph, is inevitably reduced due to the effects of lateral tire force components on the longitudinal dynamics of the vehicle. The lateral tire forces present dragging forces, which are compensated for by the speed controller's action on the drive train. To reduce the effect of the speed restoring action of the speed controller on the lateral response, the total drive torque has been limited to 500 Nm. However, in some traction control systems, the base torque is actively reduced to limit the approach of the system to instability. Such an approach would be a logical addition to the torque management controller, but is neglected here to maintain focus on the predictive torque distribution control.

Figures 5-7 show the performance of the predictive torque distribution controller presented in this paper. The on-line computed constraints, which include the corrective yaw moment and the total base torque (from a PI speed controller) during this maneuver, are shown in Figure 5.

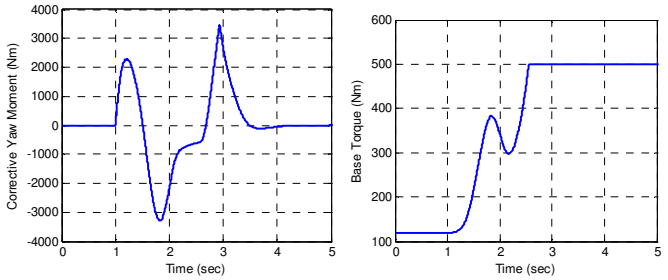

Figure 5. Constraints From an Example Torque Distribution Control

The yaw response and controlled wheel torques are shown in Figure 6. It can be seen that the actual yaw rate (solid line) follows the desired yaw rate (generated by a reference generator (Appendix), dashed line), through corrective driving and braking actions on the individual wheels.

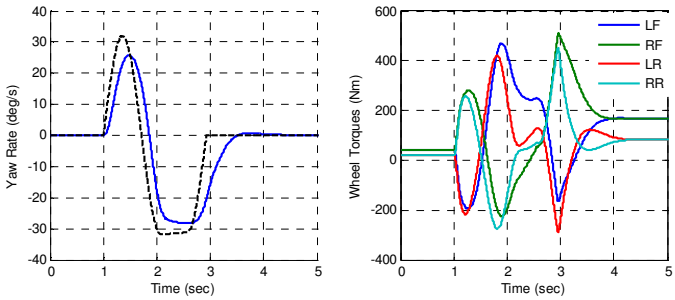

Figure 6. Yaw Rate Response and Optimal Torque Distribution

The sideslip and lateral acceleration responses under the predictive torque distribution control are shown in Figure 7. The side-slip reaches a peak of 10 degrees at its most extreme point during the maneuver, which occurs during the dwell portion of the steering input. The sideslip maintains a stable response by returning to zero with no overshoot. The lateral acceleration also approaches a peak during the dwell, late in the maneuver. The peak lateral acceleration of approximately 0.6 Gs is typical of a heavy truck, because of the significance of

lateral load transfer and it's corresponding reduction in tire lateral force capability.

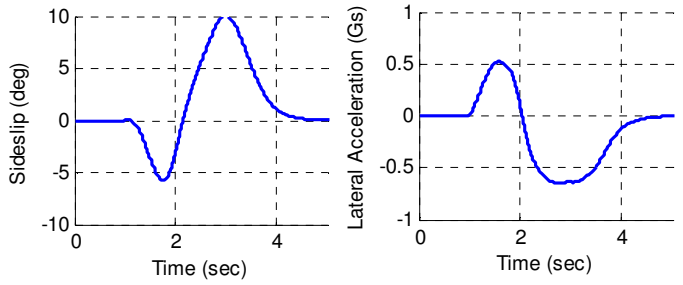

Figure 7. Side-Slip and Lateral Acceleration of Controlled Response

The above responses show that the predictive torque distribution controller performs well in maintaining the stability of the vehicle while satisfying the on-line constraints and accommodating responsiveness to driver intentions.

To further illustrate the benefits of the predictive torque distribution control strategy proposed here, its performance is compared to that of a conventional rule-based braking strategy that includes individual wheel braking and an anti-lock braking system (ABS). The rule-based braking strategy uses sequential braking as shown in Figure 8, leading to much higher torques and even requires the engagement of ABS because of wheel lock at the right rear wheel.

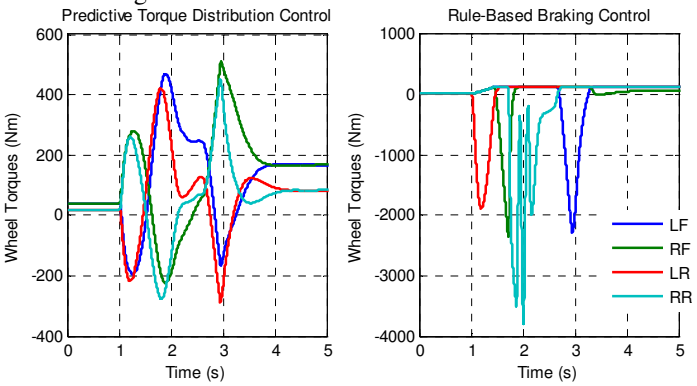

Figure 8. Comparison of Wheel Torques

The predictive torque distribution control maintains control of the vehicle within a torque range from -300 to 500 Newton meters, while the rule-based braking requires ten times the braking torques to achieve stability, but falls short of the desired corrective yaw moment. Since longitudinal forces are physically limited by the available traction of the braked tire, such rule-based braking controllers have lower instability thresholds where not enough corrective yaw moment would be generated to stabilize the vehicle. The high braking torques of the rule-based braking control push the vehicle tires to their adhesion limits, leading to much higher levels of tire saturation as seen in Figure 9.

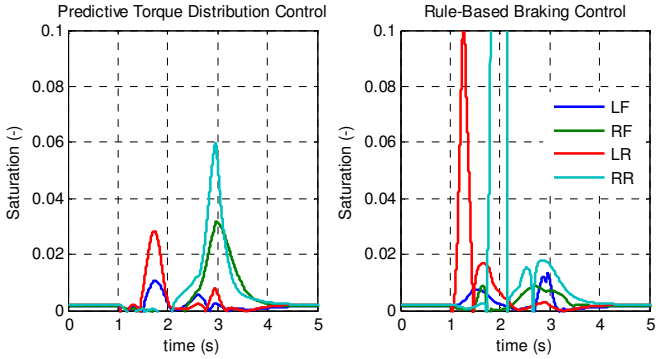

Figure 9. Comparison of Longitudinal Tire Saturations

The right rear longitudinal tire saturation of the rule-based braking control actually peaks at a value of 1.5 (indicating wheel lockup), but is not shown here for purposes of similarly scaled comparisons. Another deficiency of the rule-based braking control is that it acts counter to the speed controller by applying the brakes and reducing the velocity of the vehicle (the speed controller attempts to compensate by applying more drive torque). The predictive torque distribution control is smarter by including a constraint on achieving the demanded torque in deciding how to stabilize the vehicle.

Finally, we remark that the above results show a successful implementation of a novel predictive torque distribution control that manages longitudinal tire force saturations as the low level controller in a cascade structure featuring an already established high level yaw moment controller. The predictive torque distribution controller presented here is modular (self contained) and can be used in conjunction with any selected high-level control algorithm for corrective yaw moment generation.

SUMMARY AND CONCLUSIONS

In this paper, a new predictive torque distribution control that manages the longitudinal tire-force saturations has been proposed and described in detail. This has then been implemented in a cascading design that exploits the natural timescale separation of the lateral handling dynamics and the dynamics of the tire/wheel. Application of the proposed strategy to a two-axled heavy truck with an independent drive powertrain showed clear benefits in maintaining low longitudinal saturation levels across all tires with low drive/brake torque demands as compared to a conventional VSC strategy that employs rule-based braking to stabilize the vehicle.

To summarize, the main contributions of this paper include:

- Nonlinear tire saturations are used in a predictive framework to manage torque distribution while controlling the lateral dynamics of the vehicle.
- The predictive torque distribution control strategy solves the over actuation problem of advanced power trains with independent drives.

Finally, we note that the low level predictive torque distribution control is modular and can be interfaced with various high level controllers in the cascading structure. In our future work, we describe a cascading predictive control strategy that manages combined tire-force saturations for the purposes of vehicle stability control.

REFERENCES

1. VanZanten, T., *Bosch ESP Systems: 5 Years of Experience*, in *SAE Automotive Dynamics & Stability Conference, SAE paper number 2000-01-1633*. 2000: Troy, MI.
2. *Federal Motor Vehicle Safety Standards: Electronic Stability Control Systems, Final Rule*, N.H.T.S. Adminstration, Editor. 2007. p. 49 CFR Parts 571 and 585,.
3. Tseng, H.E., et al., *The development of vehicle stability control at Ford.* Mechatronics, IEEE/ASME Transactions on, 1999. **Vol. 4**(No. 3): p. 223-234.
4. Ghoneim, Y., et al., *Integrated Chassis Control System to Enhance Vehicle Stability.* International Journal of Vehicle Design, 2000. **Vol. 23**: p. 124-144.
5. Hac, A. and M. Bodie, *Improvements in Vehicle Handling Through Integrated Control of Chassis Systems.* Int. J. of Vehicle Autonomous Systems, 2002. **Vol. 1**(No. 1): p. 83-110.
6. J. Ackermann, T. Bunte, and D. Odenthal, *Advantages of Active Steering for Vehicle Dynamics Control*. 1999, German Aerospace Center, D.
7. Avesta Goodarzi, E.E., *Design of a VDC System for All-Wheel Independent Drive Vehicles.* IEEE/ASME TRANSACTIONS ON MECHATRONICS, December 2007. **VOL. 12, NO. 6**.
8. E. Esmailzadeh , A.G., G.R. Vossoughi, *Optimal yaw moment control law for improved vehicle handling.* Mechatronics, 2003. **Vol.13, Issue 7** p. 659-675.
9. Esmailzadeh, E., A. Goodarzi, and G.R. Vossoughi, *Directional stability and control of four-wheel independent drive electric vehicles.* Proc Instn Mech Engrs Part K: J Multi-body Dynamics. **Vol 216**.
10. Sampson, D.J.M., *Active Roll Control of Articulated Heavy Vehicles*, in *Engineering*. 2000, Cambridge University.
11. Tibaldi, M. and E. Zattoni. *Robust control of active suspensions for high performance vehicles*. in *Industrial Electronics, 1996. ISIE '96., Proceedings of the IEEE International Symposium on*. 1996.
12. Sill, J. and B. Ayalew, *Managing Axle Saturation for Vehicle Stability Control with Independent Wheel Drives*, in *American Controls Conference*, IEEE, Editor. 2011: San Francisco, CA.
13. Limroth, J., *Real-time Vehicle Parameter Estimation and Adaptive Stability Control*, in *Automotive Engineering*. 2009, Clemson University: Clemson, SC.
14. Borrelli, F., et al., *An MPC/Hybrid System Approach to Traction Control.* IEEE Trans. Control System Technology, 2006. **14**(No. 3): p. pp. 541-552.
15. Falcone, P., et al., *Predictive Active Steering Control for Autonomous Vehicle Systems.* Control Systems Technology, IEEE Transactions on, 2007. **Vol. 15**(No. 3): p. 566-580.
16. Lee, J.-H. and W.-S. Yoo, *An improved model-based predictive control of vehicle trajectory by using nonlinear function.* Journal of Mechanical Science and Technology, 2009. **23**(4): p. 918-922.
17. Falcone, P., et al. *A linear time varying model predictive control approach to the integrated vehicle dynamics control problem in autonomous systems*. 2008. Piscataway, NJ, USA: IEEE.
18. HongLiang, Z. and L. ZhiYuan. *Design of vehicle yaw stability controller based on model predictive control*. in *Intelligent Vehicles Symposium, 2009 IEEE*. 2009.
19. Falcone, P., et al., *MPC-based yaw and lateral stabilisation via active front steering and braking*. Vehicle System Dynamics: International Journal of Vehicle Mechanics and Mobility, 2008. **Vol. 46**(No. 1 supp 1): p. 611 - 628.
20. Marami, B. and M. Haeri, *Implementation of MPC as an AQM controller.* Computer Communications. **33**(2): p. 227-239.
21. Maciejowski, J.M., ed. *Predictive Control with Constraints*. 2002, Prentice Hall: Harlow, England.
22. Gawthrop, P.J. and L. Wang, *Intermittent predictive control of an inverted pendulum.* Control Engineering Practice, 2006. **14**(11): p. 1347-1356.
23. Templeton, T., et al. *Autonomous Vision-based Landing and Terrain Mapping Using an MPC-controlled Unmanned Rotorcraft*. in *Robotics and Automation, 2007 IEEE International Conference on*. 2007.
24. Sehyun, C. and T.J. Gordon, *Model-based predictive control of vehicle dynamics.* International Journal of Vehicle Autonomous Systems, 2007. **5**(1-2): p. 3-27.
25. Borrelli, F., et al., *On the computation of linear model predictive control laws.* Automatica. **46**(6): p. 1035-1041.
26. Sill, J. and B. Ayalew, *Saturation Balancing Control for Enhancing Dynamic Stability of Vehicles with Independent Wheel Drives*, in *SAE World Congress*, SAE, Editor. 2011: Detroit, MI.
27. Sill, J., S. Molla, and B. Ayalew, *Modeling and control of handling dynamics for a hydrostatically driven vehicle.* International Journal of Heavy Vehicle Systems, 2010.
28. Karogal, I. and B. Ayalew, *Independent Torque Distribution Strategies for Vehicle Stability Control.* SAE paper number 2009-01-0456, 2009.
29. Osborn, R.P. and T. Shim, *Independent Control of All-Wheel-DriveTorque Distribution.* SAE paper number 2004-01-2052, 2004.

30. Rajamani, R., *Vehicle Dynamics and Control*. 2006.
31. Astrom, K. and B. Wittenmark, *Computer Controlled Systems - Theory and Design*. Prentice Hall Information and System Science Series, ed. T. Kailath. 1997, Upper Saddle River, NJ: Tom Robbins.

APPENDICES

Established Yaw Moment Controller

The high-level feedback stability controller with an explicitly defined corrective yaw moment (of a PID type as in [4, 28-30]) compares the desired yaw rate to the actual or measured yaw rate of the vehicle to determine if the vehicle has excessive or insufficient yaw rate (over or under-steer). If excessive yaw rate error is observed, the stability controller acts to reduce the yaw rate error by requesting an effective corrective yaw moment given by:

$$M_{\psi} = \left(K_p + \frac{K_I}{s} + K_D s \right) \left(\dot{\psi}_{\text{desired}} - \dot{\psi} \right) \tag{A.1}$$

where, $\dot{\psi}_{\text{desired}} = \dfrac{V_x \delta}{L + (K_{us} V_x^{\,2})/g}$ is a desired yaw rate from a linear steady state projection from the 2 DOF model.

Linearization of Prediction Model

The longitudinal dynamics of the vehicle is predicted from a simplified expression that includes the longitudinal tire forces and the aerodynamic load. The expression is further simplified through linearization as:

$$\dot{V}_x = \frac{\sum_{i=LF\ldots RR} F_{x,i} - \frac{1}{2}\rho C_D A V_x^{\,2}}{m} \Rightarrow \frac{\sum_{i=LF\ldots RR} F_{x,i} - \rho C_D A V_{x,0} V_x + \frac{1}{2}\rho C_D A V_{x,0}^{\,2}}{m} \tag{A.2}$$

where, F_{xi} are the longitudinal tire forces; ρ is air density; C_D and A is the vehicle's drag coefficient and cross-sectional area; V_{x0} is the vehicle velocity at the point of linearization (determined by the current state); and V_x is the system state for velocity throughout the prediction.

In order to predict the dynamics of each wheel, the following equation is used for each of the four tires:

$$\dot{\omega}_i = \frac{T_i - F_{x,i} R_w - b_i \omega_i}{I_w} \qquad \text{for } i = LF, RF, LR, RR \tag{A.3}$$

where, T_i is the controlled torque, R_w is the tire radius, and b_i is wheel viscous damping. It should be noted that the wheel damping term was included in order to achieve a more stable prediction for the wheel dynamics subjected to the commanded wheel torque.

Since the longitudinal tire saturations include tire forces, it is desirable to formulate state equations for these forces. The longitudinal force dynamics can be constructed from the longitudinal vehicle dynamics as well as the wheel spin dynamics. Assuming the tire force is a function of both previously defined states, the tire force dynamics are given by:

$$\dot{F}_{x,i} = \frac{\partial F_{x,i}}{\partial \sigma_i}\frac{\partial \sigma_i}{\partial \omega_i}\dot{\omega}_i + \frac{\partial F_{x,i}}{\partial \sigma_i}\frac{\partial \sigma_i}{\partial V_x}\dot{V}_x = K_{1,i}\dot{\omega}_i + K_{2,i}\dot{V}_x \tag{A.4}$$

where the coefficients K_1 and K_2 are determined from a nonlinear representation of the tire properties from the force/slip curve and partial derivatives of the slip ratio expressions, which are analytically determined by:

$$\frac{\partial \sigma_i}{\partial \omega_i} = \frac{\partial}{\partial \omega_i}\left(\frac{\omega_i R_w - V_x}{V_x} \right)\Bigg|_{x0} = \frac{R_w}{V_{x,0}} \tag{A.5}$$

$$\frac{\partial \sigma_i}{\partial V_x} = \frac{\partial}{\partial V_x}\left(\frac{\omega_i R_w - V_x}{V_x} \right)\Bigg|_{x0} = -\frac{\omega_{i,0} R_w}{V_{x,0}^{\,2}} \tag{A.6}$$

where, $V_{x,0}$ and $\omega_{i,0}$ are the states at the point of linearization, which are defined by the current estimated values at the start of the prediction horizon. The point of linearization is also used to select the proper gradient of tire force to slip ratio, which is a form of effective slip stiffness at the linearization point. This can be implemented using a simple lookup table based on current estimates of tire slip ratio.

The tire properties contained in the lookup table are to be obtained from tire test data. However, this information would be dependent on environmental conditions that could alter the coefficient of friction between the tire and road surface. For simplicity of presenting the control structure, in this research it will be assumed that the interface between the tire and the road is similar to that of tire testing conditions. However, in practical use it is envisioned that the accuracy of the tire characteristics can be improved through a separate online friction coefficient estimator.

Substituting the derived terms from slip ratio (A.5 & A.6) as well as the wheel-spin dynamics (A.3) and the longitudinal vehicle dynamics (A.2) into the tire force equations (A.4), the state dynamics of the four tire forces are defined by:

$$\dot{F}_{x,i} = \frac{\partial F_{x,i}}{\partial \sigma_i}\left(\frac{R_w}{V_{x,0}} \right)\left(\frac{T_i - F_{x,i} R_w - b_i \omega_i}{I_w} \right) + \frac{\partial F_{x,i}}{\partial \sigma_i}\left(-\frac{\omega_{i,0} R_w}{V_{x,0}^{\,2}} \right)\left(\frac{\sum_{i=LF\ldots RR} F_{x,i} - \rho C_D A V_{x,0} V_x - \frac{1}{2}\rho C_D A V_{x,0}^{\,2}}{m} \right) \tag{A.7}$$

The equations (A.2), (A.3), and (A.7) can be placed in a state-space matrix form to be used as the linearized predictive model. The continuous state-space system is represented below in (A.9) due to equation size.

To complete the state-space output equations, the longitudinal saturations, (1), can be determined from the states of this predictive model. The defining equations of the saturations are linearized at the current states as follows:

$$\kappa_i = \sigma_i - \frac{F_{x,i}}{C_{x,i}} = \frac{\omega_i R_w - V_x}{V_x} - \frac{F_{x,i}}{C_{x,i}}$$
$$\Rightarrow \kappa_i = -\frac{\omega_{i,0} R_w}{{V_{x,0}}^2} V_x + \frac{R_w}{V_{x,0}} \omega_i - \frac{1}{C_{x,i}} F_{x,i} + \frac{\omega_{i,0} R_w - V_{x,0}}{V_{x,0}} \quad \text{(A.8)}$$

The matrix forms of the state-space and output equations are given by:

$$\begin{Bmatrix} \dot{V}_x \\ \dot{\omega}_{LF} \\ \dot{\omega}_{RF} \\ \dot{\omega}_{LR} \\ \dot{\omega}_{RR} \\ \dot{F}_{x,LF} \\ \dot{F}_{x,RF} \\ \dot{F}_{x,LR} \\ \dot{F}_{x,RR} \end{Bmatrix} = \begin{bmatrix} -\frac{\rho C_D A V_{x,0}}{m} & 0 & 0 & 0 & 0 & \frac{1}{m} & \frac{1}{m} & \frac{1}{m} & \frac{1}{m} \\ 0 & -b/I_w & 0 & 0 & 0 & -R_w/I_w & 0 & 0 & 0 \\ 0 & 0 & -b/I_w & 0 & 0 & 0 & -R_w/I_w & 0 & 0 \\ 0 & 0 & 0 & -b/I_w & 0 & 0 & 0 & -R_w/I_w & 0 \\ 0 & 0 & 0 & 0 & -b/I_w & 0 & 0 & 0 & -R_w/I_w \\ 0 & 0 & 0 & 0 & 0 & K_{21}/m - K_{11}R_w/I_w & 0 & 0 & 0 \\ 0 & 0 & 0 & 0 & 0 & 0 & K_{22}/m - K_{12}R_w/I_w & 0 & 0 \\ 0 & 0 & 0 & 0 & 0 & 0 & 0 & K_{23}/m - K_{13}R_w/I_w & 0 \\ 0 & 0 & 0 & 0 & 0 & 0 & 0 & 0 & K_{24}/m - K_{14}R_w/I_w \end{bmatrix} \begin{Bmatrix} V_x \\ \omega_{LF} \\ \omega_{RF} \\ \omega_{LR} \\ \omega_{RR} \\ F_{x,LF} \\ F_{x,RF} \\ F_{x,LR} \\ F_{x,RR} \end{Bmatrix}$$
$$+ \begin{bmatrix} 0 & 0 & 0 & 0 \\ 1/I_w & 0 & 0 & 0 \\ 0 & 1/I_w & 0 & 0 \\ 0 & 0 & 1/I_w & 0 \\ 0 & 0 & 0 & 1/I_w \\ K_{11}/I_w & 0 & 0 & 0 \\ 0 & K_{12}/I_w & 0 & 0 \\ 0 & 0 & K_{13}/I_w & 0 \\ 0 & 0 & 0 & K_{14}/I_w \end{bmatrix} \begin{Bmatrix} T_{LF} \\ T_{RF} \\ T_{LR} \\ T_{RR} \end{Bmatrix} + \begin{bmatrix} \frac{1}{2}\rho C_D A {V_{x,0}}^2 \\ 0 \\ 0 \\ 0 \\ 0 \\ 0 \\ 0 \\ 0 \\ 0 \end{bmatrix} \quad \text{(A.9)}$$

$$\begin{Bmatrix} \kappa_{LF} \\ \kappa_{RF} \\ \kappa_{LR} \\ \kappa_{RR} \end{Bmatrix} = \begin{bmatrix} -\frac{\omega_{LF,0} R_w}{{V_{x,0}}^2} & \frac{R_w}{V_{x,0}} & 0 & 0 & 0 & -\frac{1}{C_{x,LF}} & 0 & 0 & 0 \\ -\frac{\omega_{RF,0} R_w}{{V_{x,0}}^2} & 0 & \frac{R_w}{V_{x,0}} & 0 & 0 & 0 & -\frac{1}{C_{x,RF}} & 0 & 0 \\ -\frac{\omega_{LR,0} R_w}{{V_{x,0}}^2} & 0 & 0 & \frac{R_w}{V_{x,0}} & 0 & 0 & 0 & -\frac{1}{C_{x,LR}} & 0 \\ -\frac{\omega_{RR,0} R_w}{{V_{x,0}}^2} & 0 & 0 & 0 & \frac{R_w}{V_{x,0}} & 0 & 0 & 0 & -\frac{1}{C_{x,RR}} \end{bmatrix} \begin{Bmatrix} V_x \\ \omega_{LF} \\ \omega_{RF} \\ \omega_{LR} \\ \omega_{RR} \\ F_{x,LF} \\ F_{x,RF} \\ F_{x,LR} \\ F_{x,RR} \end{Bmatrix} + \begin{bmatrix} \frac{\omega_{LF,0} R_w - V_{x,0}}{V_{x,0}} \\ \frac{\omega_{RF,0} R_w - V_{x,0}}{V_{x,0}} \\ \frac{\omega_{LR,0} R_w - V_{x,0}}{V_{x,0}} \\ \frac{\omega_{RR,0} R_w - V_{x,0}}{V_{x,0}} \end{bmatrix} \quad \text{(A.10)}$$

For clarity in the continuing derivations of the predictive control, these state-matrix equations are compactly written in the form:

$$\dot{x}_c = A_c x_c + B_{1,c} u_c + B_{2,c} \quad \text{(A.11)}$$
$$y_c = C x_c + E_1 \quad \text{(A.12)}$$

where, B_1 is the input matrix corresponding to the wheel torques and B_2 is the constant term needed to account for the aerodynamic drag term appearing in (A.2).

The continuous system defined by the state-space matrices in (A.9) must be discretized at a time step, τ, of 1 millisecond so that it can be used in a predictive controller. This is accomplished through [31]:

$$A = e^{A_c T}$$

$$[B_1 \quad B_2] = \left(\int_0^T e^{A_c \tau} d\tau \right) [B_{1,c} \quad B_{2,c}] = A_c^{-1}(A - I)[B_{1,c} \quad B_{2,c}] \tag{A.13}$$

Then the resulting equivalent discrete time system is given by:

$$x_{k+1} = Ax_k + B_1 u_k + B_2 \tag{A.14}$$

$$y_k = Cx_k + E_1 \tag{A.15}$$